Influence of screening on the superconductive transition temperature

R. J. Soulen, Jr.* and M. S. Osofsky
Code 6340, Naval Research Laboratory, Washington, D.C. 20375, USA

L. D. Cooley
Materials Science Department, Brookhaven National Laboratory, Upton, New York 11973, USA
(Received 17 December 2002; published 9 September 2003)

We extend the Morel-Anderson model, originally developed to account for the superconductive transition temperature, T_c, of the elements, so that it accounts for the complete phase line for T_c of disordered systems over the full range of metallic behavior, from the pure metal to the extinction of the metallic state at the metal-insulator transition. The cornerstone of this model is the calculation of the BCS interaction potential, V, and the single-particle density of states, N, using the Landau theory for interacting fermions evaluated with a screened Coulomb interaction potential. Thus, an interpolation is established between Fermi liquid behavior and the critical regime where disorder and Coulomb interactions define the metal-insulator transition. Experimental values for T_c, N, and V were compared with these predictions and the agreement was excellent. Furthermore, since the model is expressed entirely in terms of parameters that may be calculated or measured, it has predictive powers that may prove useful in the search for high-T_c materials.

DOI: 10.1103/PhysRevB.68.094505 PACS number(s): 74.20.−z, 74.25.Dw, 74.62.−c

I. INTRODUCTION

Superconductivity is a rather ubiquitous phenomenon. It appears in 27 of the elements in bulk form and at ambient pressure (see Table I), in literally thousands of alloys,[1] in several organic conductors,[2] in many conducting oxides (including the high T_c materials),[3] in a few semiconductors,[4] and in C_{60}.[5]

The most prominent characteristic that distinguishes one superconductor from another is the superconductive transition temperature, T_c. It was recognized early on—indeed by the very discoverer of the phenomenon, H. K. Onnes—that there were practical ramifications of superconductivity. For example, Onnes inferred that one characteristic of the superconducting state, the ability to carry current without loss, could be used to generate magnetic fields. He also appreciated the fact that a higher value of T_c would reduce the burden and expense of providing the requisite cryogenic environment. Thus the ''search for high-T_c superconductivity'' began with Onnes in 1911 and continues unabated today.

Eventually all of the elements were examined for the presence of superconductivity. A summary of the results is presented in Table I. The entries indicate clearly that elemental superconductivity is a decidedly low-temperature phenomenon: The highest T_c (for Nb) is only 9.3 K. Thus the search for higher-T_c superconductivity inevitably widened to include alloys of the form $A_{1-x}B_x$, where x is the concentration of B atoms in the host lattice of A atoms (shorthand notation, A-B). The purpose of the alloying was to increase T_c above that of the host. The following observations may be distilled from these extensive studies.

(1) For many systems, as the disorder was increased by doping, radiation damage, and other means, or as the carrier concentration was decreased, the electrical conductivity σ decreased until the system became insulating, i.e., $\sigma(T \rightarrow 0)=0$. This point is identified as the metal-insulator transition (MIT).

(2) The measured values of T_c as a function of x define the phase line $T_c(x)$ that separates the normal and superconducting phases. When $T_c(x)$ was measured for systems with a MIT, the behavior fell into one of two categories: either there was no enhancement above that of the host and T_c gradually decreased until it disappeared at the MIT, or T_c increased above the host to a maximum and then decreased until it vanished at the MIT.

(3) Figure 1, which shows T_c as a function of the distance from the MIT for nine systems, indicates that the behavior is actually continuous between these two limits. Irradiated Nb_3Sn is an example of the former limit, whereas the remaining eight curves are arranged to illustrate the behavior as the enhancement becomes progressively larger.

The search for enhanced superconductivity has been and is still carried out for the most part without the benefit and guidance of a firm theoretical framework. Instead, various empirical correlations (such as T_c versus electron-to-atom ratio[6] e/a or versus the residual resistance ratio[7]) have been noted and used with moderate success. Alternatively, band theory can be used to estimate T_c on a case-by-case basis. The purpose of this article is to present a simple model for T_c that is applicable for the whole conductivity range from the pure metal to the MIT. This model is an extension of the approach of Morel and Anderson[8] (MA), in which T_c for many of the elements was calculated within the framework of the Eliashberg formulation of superconductivity using a screened Coulomb potential for the interaction between the electrons. The extension presented here, dubbed the extended Morel-Anderson (EMA) model, is based on the recent observation by Osofsky *et al.*[9] that screening also plays a crucial role in metals near the MIT. In that first examination, several systems, such as WSi shown in Fig. 1, where T_c for the pure metal is nearly zero, were successfully described by the first version of the EMA model. In this article we generalize the model using the Eliashberg formulation in a way that encompasses the remaining cases shown in Fig. 1, where T_c for the

TABLE I. Properties of the superconducting elements.

Element	γ (mJ mol^{-1} K^{-2})	Θ_D (K)	T_c (K)	N_0 (states eV^{-1})	k_{TF} (Å^{-1})	λ	μ^*	q_c (Å^{-1})	$V_{0\mathrm{exp}}$ (eV)	$V(0)$ (eV)
Al	1.36	4230	1.20	0.28	0.50	0.34	0.17	0.69	1.20	1.83
Be	0.16	1,480	0.02	0.03	0.17	0.26	0.17	0.28	7.98	10.90
Cd	0.67	252	0.56	0.14	0.35	0.34	0.17	0.49	2.39	3.63
Ga	0.60	317	1.09	0.12	0.33	0.35	0.17	0.45	2.75	4.23
Hf	2.40	256	0.09	0.50	0.66	0.30	0.17	1.02	0.59	0.84
Hg	2.20	75	4.15	0.46	0.63	0.52	0.15	0.61	1.11	2.32
In	1.70	109	3.40	0.36	0.56	0.46	0.16	0.60	1.28	2.36
Ir	3.15	425	0.10	0.66	0.76	0.29	0.17	1.18	0.44	0.62
La	10.10	142	4.90	2.14	1.36	0.47	0.16	1.45	0.22	0.41
Mo	2.10	459	0.92	0.44	0.62	0.33	0.17	0.87	0.75	1.13
Nb	7.66	277	9.26	1.62	1.19	0.46	0.16	1.27	0.28	0.53
Os	2.35	500	0.66	0.49	0.65	0.32	0.17	0.94	0.65	0.96
Pb	3.14	102	7.23	0.66	0.76	0.55	0.14	0.68	0.82	1.84
Re	2.40	415	1.70	0.50	0.66	0.35	0.17	0.89	0.69	1.08
Rh	4.60	480	(370 μK)	0.98	0.92	0.22	0.15	1.73	0.22	0.29
Ru	3.30	600	0.51	0.70	0.78	0.31	0.17	1.15	0.45	0.65
Sn	1.78	196	3.72	0.37	0.57	0.43	0.16	0.66	1.14	2.00
Ta	5.84	258	4.48	1.24	1.04	0.42	0.16	1.22	0.33	0.58
Tc	4.06	351	7.77	0.86	0.86	0.44	0.16	0.97	0.51	0.91
Th	4.69	170	1.37	0.99	0.93	0.38	0.17	1.19	0.38	0.61
Ti	3.41	426	0.39	0.72	0.79	0.31	0.17	1.17	0.43	0.63
Tl	2.83	88	2.36	0.60	0.72	0.45	0.16	0.79	0.75	1.36
U	10.90	200	1.10	2.31	1.42	0.36	0.17	1.87	0.15	0.24
V	9.04	399	5.38	1.92	1.29	0.40	0.16	1.56	0.21	0.36
W	1.22	388	0.014	0.25	0.47	0.27	0.17	0.78	1.04	1.43
Zn	0.64	316	0.875	0.13	0.34	0.34	0.17	0.47	2.54	3.88
Zr	2.91	289	0.520	0.61	0.73	0.33	0.17	1.03	0.54	0.81

pure metal is not zero. Furthermore, in this article we document the remarkable success of the EMA model in accounting for a broad range of experimental data.

The organization of the remainder of this article is as follows: In Sec. II, a coordinate is introduced that measures the distance from the MIT and the three ranges of metallic behavior are identified and placed upon this axis. The MA model will be reviewed for the elements in Sec. III A, while its extension to disordered metals is given in Sec. III B. The model for disordered metals is compared with data for several systems drawn from the literature in Sec. IV. Analysis and interpretation of the results appear in Sec. V. Section VI reports the conclusions. Appendix A provides the detailed calculations that lead to the results discussed in Sec. III A, while Appendix B provides the analogous support for Sec. III B. In Appendix C, the results from Appendixes A and B are combined into a single model that spans the full metallic range. Appendix D indicates how the EMA model can account for several, decades old, unexplained correlations between superconductivity and measured quantities.

II. RANGE OF METALLIC BEHAVIOR

On the metallic side of the MIT, transport behavior can be divided into three regimes that correspond to three different conductivity ranges. The first begins at the pure (very clean) limit where the appropriate description of physical behavior is given in terms of an uncorrelated Fermi liquid, comprised of long-lived, weakly interacting carriers (quasiparticles) occupying well-defined energy and momentum states. This description still remains valid for imperfections at low and moderate concentrations, for moderate electron-electron interactions, or for small depletions of the carrier concentration. We refer to this latter region as the correlated Fermi liquid region, and we identify the complete range, uncorrelated and correlated, as the Fermi liquid region (FLR). In this region physical laws for transport are given by kinetic theory for quasiparticles governed by Boltzmann transport.

As the disorder or the interaction strength between carriers is further increased or the carrier concentration is decreased, however, the concept of a Fermi liquid becomes increasingly inaccurate. Consequently, many of the concepts and concomitant equations representing the behavior of the normal and superconducting states are rendered invalid. We identify this region as the ''precritical region'' (PCR) where fluctuations begin to become important. Finally, when the disorder is sufficiently large to induce fluctuations on a length scale comparable with the thermal diffusion length, the system enters the ''critical'' region (CR), very analogous to critical opalescence encountered in other phase transitions. In this region, fluctuations are so large that the quasiparticle

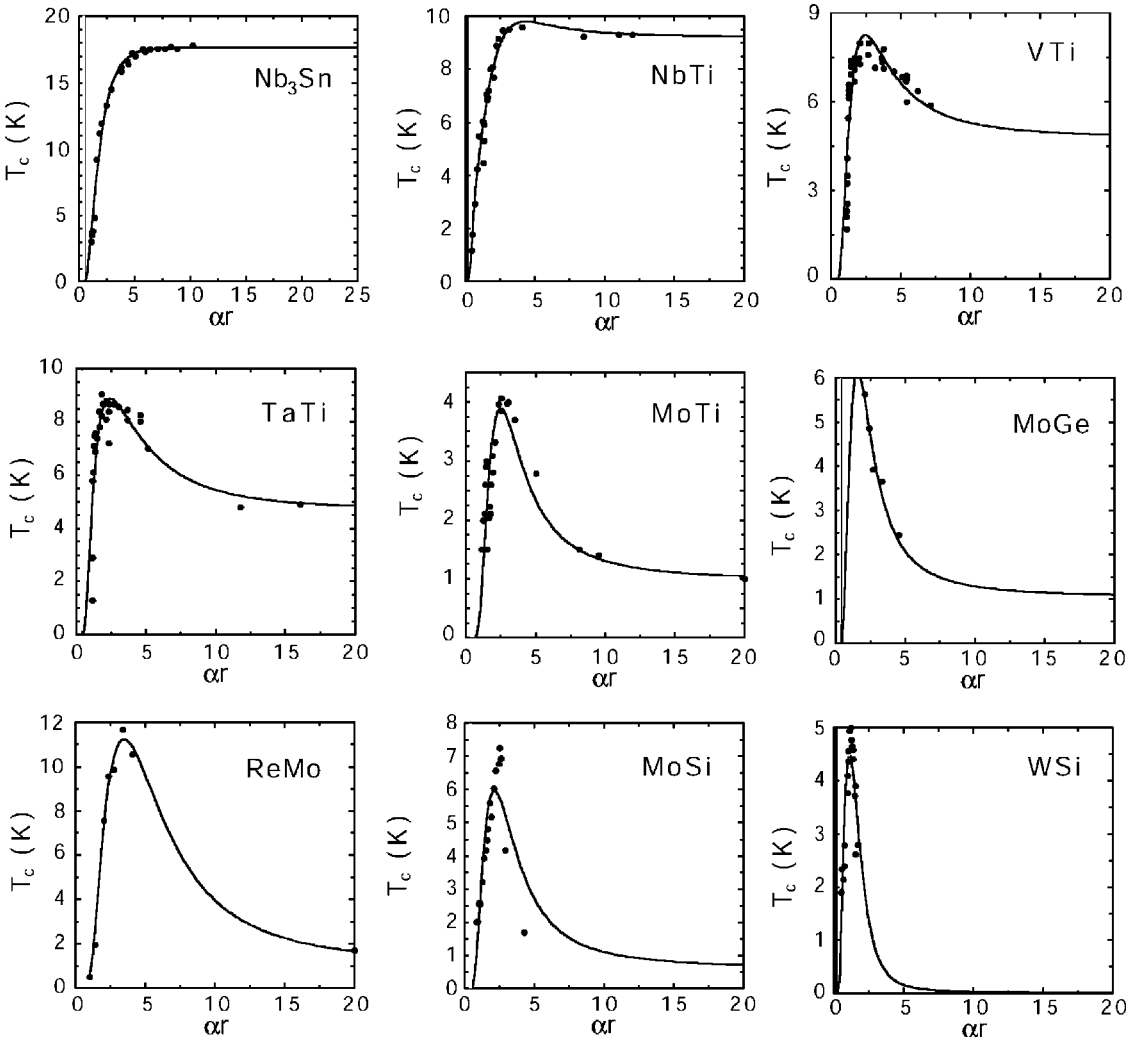

FIG. 1. The superconductive transition temperature, T_c, as a function of distance, αr, from the metal-insulator transition ($\alpha r=0$) for nine alloy systems. The data points are shown as solid circles, and the solid curves represent fits to the data using a model presented in the text. The fitting parameter, a, whose magnitude quantifies the extent of the T_c enhancement, is given in parentheses for each system: Nb_3Sn (0.01), Nb-Ti (0.69), V-Ti (1.5), Ta-Ti (2.5), Mo-Ti (6.), Mo-Ge (15), Re-Mo (11), Mo-Si (17), and W-Si (24.1).

concept is totally without validity, and physical properties are instead rigorously described by scaling laws.

The first step in building a description of T_c over the full range of metallic behavior is to introduce a coordinate that defines the ''distance'' from the MIT. The appropriate choice is the inverse of the correlation length, $1/\xi$,[10] which in turn is defined in terms of a measured quantity p. For instance, p may be the carrier concentration, n, or the doping concentration, x, or $\sigma_{300\,\mathrm{K}}$, the value of the conductivity at 300 K (see Osofsky *et al.*[11]). By definition, $1/\xi \sim [(p-p_c)/p_c]$, where p_c is the value of p at the MIT. The expression for $1/\xi$ may be written more precisely as

$$\frac{1}{\xi}=\left(\frac{\alpha}{a}\right)^{1/\nu}\left(\frac{p-p_c}{p_c}\right)^{1/\nu}=\left(\frac{\alpha r}{a}\right)^{1/\nu}, \qquad (1)$$

where a is a microscopic parameter comparable to the lattice parameter, α is a constant to be determined, and the critical exponent, ν, has been shown to be approximately 1 for many systems[12] (to be discussed in more detail later). Furthermore, p_c may be determined by an experimental technique (see Ref. 9) *so that r is completely defined by experimentally measured quantities*. We may also express ξ in terms of $k_F l$, the parameter often used to quantify disorder. That is, if we identity the MIT by the condition $k_F l=\pi$, then $k_F l=r+\pi$ applies as the MIT is approached.

Having defined the proper coordinate, the three regions may be arranged in a logical order and the range of each more precisely defined. The following discussion proceeds in ascending r, beginning at the origin.

a. The critical region (CR). Here $r\sim 0$ and the thermal diffusion length at a given temperature is less than ξ. The two mechanisms most commonly thought to produce the MIT are often discussed as mutually exclusive phenomena. It is indisputable that, on one hand, disorder alone can induce the MIT in a system of noninteracting fermions (the Anderson mechanism).[13] However, since fermions also carry electrical charge, there is always a Coulomb interaction, and so the fermions may not be considered completely free after all.

Alternatively, electron interactions alone can lead to a MIT (the Mott transition).[14] However, since disorder is generally also present in real systems in the vicinity of the MIT, a pure Mott transition is generally not observed, either. For these reasons it is advisable to abandon discussions phrased simply in either of these two distinct concepts and proceed *ab initio* with a more realistic model, in which both effects, disorder and Coulomb interactions, are considered on equal footing.

Belitz and Kirkpatrick[15] have reviewed theoretical efforts to carry out such a plan. A general scaling theory of the MIT has emerged, accompanied by renormalization group calculations for the various universality classes. The conclusion is that there are at least eight universality classes for disordered, interacting fermions. These include systems with one of four symmetry-breaking mechanisms (magnetic impurities, magnetic field, spin-orbit coupling, or none), each with either short-range (SR) or long-range (LR) interactions. In all cases, various physical quantities obey universal scaling equations as a function of ξ. Thus, in particular,

$$\sigma = \sigma_a \left(\frac{a}{\alpha \xi} \right)^{\nu(d-2)}, \tag{2a}$$

$$N(0) = N_a \left(\frac{a}{\alpha \xi} \right)^{\delta}, \tag{2b}$$

where ν and δ are specified for each class and d is the sample dimension. For example, for a three-dimensional, spin-orbit coupled system with a Coulomb interaction, the prediction is that $\nu=1$ and $\delta=2$. When, however, experiments were carried out on three systems for which these conditions should definitely hold [Mo_xGe_{1-x} (Ref. 16), Nb_xSi_{1-x} (Ref. 17), and $Si_{1-x}Au_x$ (Ref. 18)], the evidence was very clear that $\nu=1$ and $\delta=1$.

This discrepancy for the value of δ is worth discussing in some detail. It could be due to an inadequacy of the theory or to a problem with the experiments. Another, more probable cause must be considered: that the experiments were not in the critical region. The range of the CR is quite small, since the thermal diffusion length is generally greater than ξ. In conventional phase transitions, where the CR is also very small, the CR is accessible to experiment only by virtue of the fact that ξ is defined in terms of temperature, i.e., $\xi \propto [(T-T_c)/T_c]^{1/\nu}$, which may be controlled near T_c with very high precision. For the MIT case, however, the CR is controlled by a variable that is hard to measure and control close to the critical value. It is therefore very likely that most, if not all, of these measurements were taken under conditions placing them in a region where $\xi < L$, the precritical region (PCR), rather than in the CR. Thus we discuss the PCR next.

b. The pre-critical region (PCR). Here $\xi < L$ and $0 < r < r_0$. Strictly speaking, the scaling laws defined above, the universal critical exponents and the accompanying rules relating the critical exponents, apply only to the CR. Since, however, the fluctuations gradually decrease (rather than disappear abruptly) as the system transitions from the CR to the Fermi liquid limit, we expect that some vestige of the scaling laws should persist in the latter region. It appears prudent to adopt a nonrigorous, but reasonable position, that scaling laws still are valid for the PCR, but with ''preasymptotic'' critical exponents that are no longer governed by the theory developed for the CR. Indeed, it has been found possible to extend the scaling laws from the CR into the PCR in an approximate way by supposing that there are logarithmic corrections to scaling in the PCR.[19] Another approach is to solve the renormalization group flow equations of the MIT for the different ranges of L or ξ.[20] The PCR merges with the FLR at a value r_0, defined below.

c. The Fermi liquid region (FLR). Here $\xi \ll l_{TF}$ and $r_0 < r < \infty$. As r is increased beyond r_0, the system gradually leaves the PCR and enters the lower (impure) end of the FLR. Here the quasiparticles interact strongly as a correlated Fermi liquid, which henceforth will be called the strong limit. The superconducting properties in this subregion (see Appendix B) are quite different from the more familiar behavior of weakly interacting fermions (henceforth called the weak limit). This latter subregion, where classical Landau Fermi liquid theory applies, defines the upper (pure) region of the Fermi liquid. The properties of superconductivity in the weak limit are discussed in Appendix A.

d. Summary: *the complete metallic region.* Here $0 < r < \infty$. Thus the coordinate axis, r, extends from 0 to infinity and is broken up into three regions. The CR extends for only a short distance from $r=0$ for macroscopic samples and thus occupies only a small fraction of the r axis. As r increases, the system transforms smoothly from the CR to first the PCR, then to the strongly interacting, correlated subregion of the FLR, and finally to the weakly interacting, uncorrelated subregion of the FLR. There are no sharp boundaries (i.e., abrupt changes in behavior) between these regions, and there are no precise theoretical definitions for the boundaries. Nevertheless, we can estimate the location of the most important boundary, at r_0, which separates the PCR and the FLR. It turns out that r_0 is rather small [see discussion of Fig. 3(b), Sec. IV], so the FLR extends over a surprisingly large region of the total coordinate axis. In Appendix C we develop a model that accounts for the complete phase diagram $T_c(r)$ over the full metallic range ($0 < r < \infty$) using functions for the quantities appearing in the expression for T_c, which span the full range.

III. MODELS FOR T_c

Accounting for superconductivity for the full metallic range is problematic because the conventional picture of long-lived quaisparticles assumed by the BCS theory or by the Eliashberg model becomes increasingly inaccurate as the MIT is approached. Thus, any model for superconductivity in this region faces this fundamental challenge. Nevertheless, scaling theories have been used to model the phase line, $T_c(x)$, separating the normal and superconducting phases of low-T_c superconductor (LTS) materials. Some could only explain the observed depression in T_c for large x, and could not account for the observed increase in T_c for small x.[21,22] Two theories predict $T_c(x)$ curves that mimic the shape of the whole phase diagram (including enhancement). The first is developed for systems with a low Fermi energy E_F, and is

thus restricted to the C_{60} and the high-T_c superconductor (HTS) systems.[23] The second is also restricted to HTS systems.[24] Furthermore, when the specific heat results were obtained for several superconducting systems, N was found to depend systematically on x. Accordingly, the calculated values of V also depended on x. Although $N(x)$ and $V(x)$ were determined for several alloy systems, Nb-Mo (Ref. 25) and Ti-Zr (Ref. 26), to name but two, their functional form was not adequately accounted for by theory. See the recent overview by Sadovskii[27] for details of these efforts. Along with these difficulties, very often the theories, derived for one of the regions, were extended without justification to another region where their applicability is very likely inappropriate.

Accordingly, we chose an alternative strategy. We developed single functions for N and V that matched the known functions for the FLR and that also satisfied the boundary condition at $r=0$ (the MIT). So constructed, these functions ''bridge'' the gap in the PCR. We start the development of these functions by reviewing the theory for the Fermi liquid region.

A. T_c for the Fermi liquid region in the weak limit

Morel and Anderson calculated the T_c values for the elements using the McMillan solution of the Eliashberg equations for T_c (see Appendix A). That is,

$$T_c = 0.85\Theta_D \exp\left[\frac{-1.04(1+\lambda)}{\lambda-\mu^*(1+0.62\lambda)}\right], \tag{3}$$

where

$$\lambda = N_0\left[\frac{4\pi e^2}{k_{TF}^2+(2k_F)^2}\right] = N_0 V_0, \tag{4a}$$

$$\mu = \ln\left[1+\frac{(2k_F)^2}{k_{TF}^2}\right] = -\ln\lambda, \tag{4b}$$

$$\mu^* = \frac{\mu}{1+\mu\ln(E_F/k_B\Theta_D)}, \tag{4c}$$

and where N_0 is the single-particle density of states, k_F the Fermi wave vector, and Θ_D the Debye temperature. Equations (4a) and (4b) were obtained by performing integrations over a spherical Fermi surface of the Fourier transform of a screened, Coulomb electrostatic potential. That is, if $V(x)=(e^2/x)\exp(-k_{TF}x)=(e^2/x)\exp(-x/l_{TF})$, then the Fourier transform $V(q,k_{TF})$ is given by

$$V(q,k_{TF}) = \frac{4\pi e^2}{q^2\epsilon(q,k_{TF})} \simeq \frac{4\pi e^2}{k_{TF}^2+q^2}. \tag{5}$$

These integrations were carried out to a maximum value q_c, which Morel and Anderson set equal to $2k_F$. Here $l_{TF}=1/k_{TF}$ is the Thomas-Fermi screening length and ϵ the dielectric function. We note that a reduction in k_{TF} reduces the dielectric constant and enhances V and thus T_c. Enhanced transition temperatures, albeit not as dramatic as these described here, have been observed in thin film normal metal/superconductor bilayers and normal metal/insulator/superconductor trilayers that have been also attributed to a reduced dielectric constant.[28,29]

Using these expressions for λ and μ^*, Morel and Anderson generated a table for several of the elements, comparing the predicted values of λ_0 with ''experimental'' values λ_0 obtained by inverting the McMillan formula and calculating λ_0 from experimental values of T_c and Θ_D. In general the agreement was rather good.

In order to establish the basis for the treatment of disordered metals given in the next section, we update and rephrase the MA work here. Instead of using λ_0, however, we factor it into N_0 and V_0. A more comprehensive version of the Morel-Anderson table, which includes all the superconductive elements, is given here as Table I. Included are measured values for the Sommerfeld constant γ, Θ_D, and T_c. From these measured quantities were calculated $N_0=0.212\gamma=(4\pi e^2)^{-1}k_{TF}^2$. The determination of λ and μ^* came from the following analysis: Using the definitions given above, we established the identity (for small λ) $\lambda-\mu^*=\lambda-[-\ln\lambda/(1-5\ln\lambda)]=1/\ln(T_c/0.855\Theta_D)$. The right-hand side of this equation was evaluated from experimental data for each element, and then the value of λ was found that satisfied this identity. Then μ and μ^* were calculated from Eqs. (4b) and (4c) using the value for λ. These data are presented in Table I. The interaction potential was then calculated using the definition, $V_{0\,expt}=[1/\ln(T_c/0.855\Theta_D)+\mu^*][1/N_0]$. We determined experimental values for q_c by using the definition, $V_{0\,expt}=(4\pi e^2)/(k_{TF}^2+q_c^2)$. The results of this calculation are also presented as a column in Table I.

It is quite illustrative to plot $V_{0\,expt}$ versus k_{TF} for all the elements to test the conformity of this quantity with the analytic form of the screened Coulomb potential. As Fig. 2(a) clearly shows, the data for $V_{0\,expt}$ (plotted points) are well represented as a function of k_{TF} by Eq. (5) (the solid line). Concerning the identity of the phonon cutoff, we tested two possible correlations for q_c: $q_c=2k_F$, suggested by Morel and Anderson and by Pines,[30] and $q_c^2=0.6q_D^2$, suggested by de Gennes,[31] where $q_D^2=(3/4\pi)^{2/3}4\pi^2/a_0^2$ and a_0 is the lattice constant for a cubic metal. Evaluating these expressions gives the simple result, $q_c a_0=3.02$. To test both correlations, the data for the calculated values of q_c were plotted versus the appropriate ordinate. The correlation defined by MA was slightly stronger than the other two, and this is the one presented in Fig. 2(b).

B. T_c for the Fermi liquid region in the strong limit

We now turn to the strong-interaction part of the FLR, where there is an adequate theory for superconductivity. In order to propose functional forms for $V(x)$ and $N(x)$, and thus T_c, we consider screening. Since the carriers become more correlated as the MIT is approached, they become less capable of responding to applied fields, resulting in increased screening lengths. We propose then that the basic equation for the screened Coulomb interaction continues to apply, but

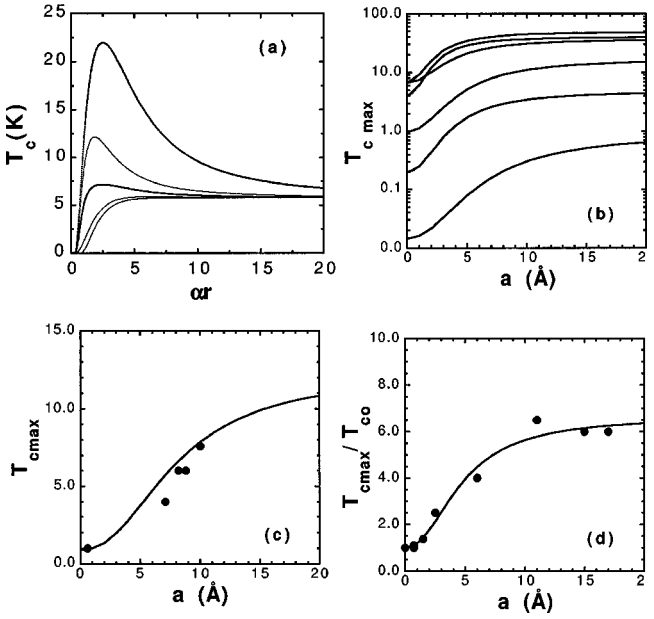

FIG. 2. (a) The experimentally determined BCS interaction potential, $V_{0\ expt}$ for all the superconducting elements (solid circles) (as given in Table I) and the alloy/disordered superconductors (open circles) (as given in Table II) as a function of the Thomas-Fermi vector, k_{TF}. The solid line represents a fit of a screened Coulomb potential (see text). (b) The phonon cutoff momentum, q_c, as a function of the Fermi wave vector, k_F. The solid curve represents a linear fit of q_c to k_F.

that the Thomas-Fermi screening length is replaced by the variable ξ, and that $k_s=1/\xi$. In support of this idea, note that in the pure limit k_s is the inverse of the screening length and is given by the Thomas-Fermi expression, $k_{TF}^2=4\pi e^2(\partial n/\partial\mu)=4\pi e^2 N_0$. As the MIT is approached, both theory[32,33] and experiments[34,35] have shown that $\partial n/\partial\mu$ is no longer constant (N_0) but decreases until it vanishes at the MIT. Alternatively then, the screening length diverges as the MIT is approached. In Appendix B we develop an explicit expression for k_s, which serves to"bridge" the two regions. Thus

$$k_s^2=4\pi e^2(\partial n/\partial\mu)\sim\frac{k_{TF}^2}{1+(a/\alpha r)^2}. \tag{6}$$

So defined, the screening length $l_s=1/k_s$ has the correct limits: l_s diverges when $r\to 0$ (the MIT), and $l_s=l_{TF}$ in the pure limit ($r\to\infty$). Accordingly, the screened potential is an extrapolation of V_0,

$$V(r)=\frac{4\pi e^2}{k_s^2+q_c^2}. \tag{7}$$

$V(r)$ for an alloy system thus starts out at the value V_0, which is characteristic of the pure host metal, and is analytically continued via the expression for r as the doping is increased. The curve for $V(r)$ in some sense recapitulates the curve given in Fig. 2(a) for the elements, but the difference is that r may be varied continuously and over a greater range.

The density of states is also changed by proximity to the MIT. In Appendix B we present an expression for N for strongly interacting fermions, and in Appendix C we develop the following bridging function, which smoothly interpolates between the MIT and the FLR:

$$N(\alpha r)=N_0[1-\exp(-\alpha r)]^\delta = N_0\left\{1-\exp\left[-\alpha\left(\frac{\sigma}{\sigma_c}-1\right)\right]\right\}^\delta, \tag{8}$$

where it is seen that $\alpha=N_a/N_0$ by using Eqs. (1) and (8) (in its limiting form near the MIT).

C. T_c for the full metallic range

Thus we have bridged the region from the pure limit to the MIT by defining appropriate functions of a coordinate defined in terms of the correlation length. The expression for T_c is given by the McMillan expression, where, for the same reasons given for the elements, $\mu^*\sim 0.15$. Hence,

$$T_c=0.85\Theta_D\exp\left[\frac{-1.04(1+\lambda)}{\lambda-0.15(1+0.62\lambda)}\right], \tag{9a}$$

$$\lambda=N_0[1-\exp(-\alpha r)]^\delta\left(\frac{4\pi e^2}{k_s^2+q_c^2}\right), \tag{9b}$$

$$k_s^2=4\pi e^2(\partial n/\partial\mu)\sim\frac{k_{TF}^2}{1+(a/\alpha r)^2}. \tag{9c}$$

We make several observations about this function. The EMA model has the proper limiting behavior. In the pure limit, i.e., for large r, Eq. (9a) reduces appropriately to $T_{c0}=0.85\Theta_D\exp(-1/N_0V_0)$. Indeed, for all the materials analyzed in this article, this equation gave the same values for the fitted parameters (to within 1%) as did Eq. (9a). Second, it disappears at the MIT ($r=0$).

The equation for T_c in the EMA model is a generalization of one developed earlier by the authors (M.O. and R.J.S.) in which screening was incorporated into a jellium model for disordered superconductors. The previous model used the definition $N\sim N_0\alpha r$, which diverges at large αr. However $V\sim 1/(\alpha r)^2$, so $\lambda\sim 0$ for large αr, which means $T_c\sim 0$ in the pure limit. Thus, our previous model could only describe those superconducting systems that satisfy the condition $T_{c0}=0$. The EMA model, however, uses Eq. (7) for V and Eq. (8) for N, which have a finite limit (λ_0 for large r) and thus permit the modeling of systems with either finite or zero T_{c0}. Stated simply, the EMA model contains the previous model as a special case. To check the equivalence of the two models for the case $T_{c0}=0$, we refitted the same data for low-T_c materials (Ref. 9) and oxide metals including the cuprates[36] with the EMA model. The fits of either model are equally good, although the fitting parameters are defined somewhat differently. One purpose of this article is to demonstrate how well the EMA model fits data for systems for

which T_{c0} is not zero, and thus many of the new data sets to be presented and analyzed in this article fall into the category of a finite T_{c0}.

The system of Eqs. (9) has only three fitting parameters: σ_c, α, and a. Fitting $N(\alpha r)$ requires the parameters N_0, σ_c, α, and δ, but the value of N_0 is known, however, from the Sommerfeld constant, and other experiments show that $\delta=1$,[12] thereby reducing the number of unknown parameters in the expression for N to two. Fitting T_c introduces the third parameter, a. The other two parameters appearing in the expression for T_c (l_{TF} and q_c) have been evaluated for the host (Table I) and are known. The expression for T_c thus contains two types of parameters. Those for the host metal (N_0, δ, l_{TF}, and q_c) are known from other experiments or from calculation. The remaining parameters (σ_c, α, and a), however, must be obtained from fitting experimental data, and they characterize the behavior of the system near the MIT. The first of these parameters (σ_c) identifies the location of the MIT on the conductivity axis, the second (α) defines the scale of the coordinate that measures the distance from the MIT, and the last parameter (a) sets the scale of the screening length. Thus the T_c for the disordered system evolves from the pure state, chiefly via the changes induced in the screening length by the disorder.

An interesting property of a system is the maximum value, $T_{c\,max}$, that T_c can attain. Empirically we find that the maximum occurs for $\alpha r \sim 3$, in which case

$$T_{c\,max}=0.85\Theta_D \exp\left[\frac{-1}{0.95N_0[4\pi e^2/(k_{sm}^2+q_c^2)]-\mu^*}\right], \tag{10a}$$

with

$$k_{sm}^2=\frac{1}{l_{TF}^2+(a/3)^2}. \tag{10b}$$

IV. EXPERIMENTAL DATA AND COMPARISON WITH THE EMA MODEL

We are interested in analyzing systems for which both T_c and N data were determined so that V could be calculated and compared with the prediction. That is, at a minimum, we need T_c as a function of σ (or of x if the relation between σ and x has been established). Furthermore, data for either γ and/or dH_{c2}/dT are needed to independently define the density of states. An additional requirement was that both sets of data should cover enough of the range from good conductor to the MIT to provide sufficient data for adequate fitting by the appropriate equations. Finally, since the model now could accommodate any value for T_{c0}, there was no restriction on its value. A search of the literature with these requirements led us to choose the following alloy systems.

Nb-Ti. Data for the $Nb_{1-x}Ti_x$ system were taken from four sources: the first set[37] (bulk samples prepared in equilibrium) covered the range $0<x<0.58$; the second set[38] (thin film samples) ranged from $0.58<x<0.87$, the third set[39] (wires) covered the range $0.60<x<0.76$, and the last set[40] (rapidly quenched bulk samples) covered the range from $0.65<x<0.99$. We found that the conductivity versus x presented in the first two references was very consistent, so that x for all the sources was readily converted into a common σ axis. For Nb-Ti, the slope of the upper critical magnetic field H_{c2} near T_c was calculated for the data sets from the first three data sets using the equation $(dH_{c2}/dT)|_{T=T_c}=H_{c2}(0)/0.69T_c$. Several slopes were measured directly in the last reference, and their values agree very well with the calculated slopes obtained from the first three. Some of the samples have normal inclusions of Ti to promote stronger flux pinning for magnet applications. However, these regions are small enough to be effectively mixed by the proximity effect, and properties comparable to the equivalent homogeneous, single-phase alloy are observed in experiments (see Ref. 37 and references therein).

Nb_3Sn and V_3Si. Data were obtained as a function of radiation damage by Ghosh and Strongin.[41] The thin film samples, prepared by *e*-beam coevaporation onto a heated single-crystal sapphire substrate, were exposed to α^{++} radiation and then T_c, resistivity ρ_0, and $(dH_{c2}/dT)|_{T_c}$ were measured as a function of dosage.

W-Si. Data for T_c, ρ_0, and $(dH_{c2}/dT)|_{T_c}$ were measured for W-Si alloys by Bond *et al.*[42] and by Kondo.[43]

Mo-Ge and Mo-Si. Data for T_c, ρ_0, and $(dH_{c2}/dT)|_{T_c}$ were measured for Mo-Ge and Mo-Si thin-film alloys by Kubo.[44]

Ti and Mo alloys. T_c, was measured versus x for Nb-Mo alloys by Hein *et al.*,[25] while γ from specific heat and T_c were determined versus x by Morin and Maita.[45] T_c, ρ_0, and $(dH_{c2}/dT)|_{T_c}$ measurements for V-Ti, Ta-Ti, and Mo-Ti alloys were described in the compendium by Collings.[46] Data on T_c, ρ_0, and $H_{c2}(0)$ for TaTi and MoTi were also given in the work of Berlincourt and Hake.[47]

An example of the first step in the data analysis carried out for each system is shown in Fig. 3(a). Here the experimentally determined density of states for Nb-Ti is plotted versus σ as well as the curve fitted by Eq. (8). In this manner, values for the parameters N_0, α, σ_c, and δ were obtained. This procedure was repeated for seven other systems where there were sufficient data to perform the fit. The values of the fitted parameters are presented in Table II. Data for three systems were suitable to use the four-parameter equation (8). The average value and standard deviation for δ for these three systems were found to be $\delta=0.99\pm0.02$. The remaining, less extensive, five sets were fitted to Eq. (8) with $\delta=1$. Other data in the literature for $N(\sigma)$ are more sparse and therefore δ could not be defined as precisely (see Ref. 9). Nevertheless, an analysis of the behavior of $N(r)$ near the MIT for four other systems led to the conclusion that $\delta=1.06\pm0.09$. Furthermore, the value $\delta=1$ was determined from measurements of the density of states of Nb_xSi_{1-x} near the MIT using tunneling.[12]

Once σ_c was defined, r was determined by Eq. (1), and $N(\sigma)$ could be reexpressed in terms of αr. The ratio, $N(\alpha r)/N_0$, for the eight systems is shown in Fig. 3(b). The solid curve represents the curve fitted to the average of the

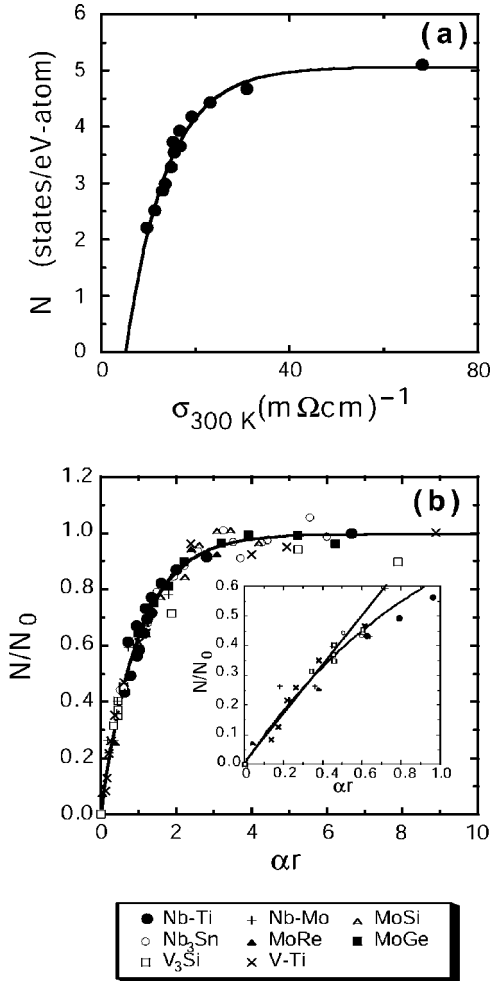

FIG. 3. (a) Plot of the density of states N for Nb-Ti (solid circles) as a function of the electrical conductivity, σ. Note that at large σ, the density of states approaches the normal-state value, N_0. (b) The ratio, N/N_0, for eight systems as a function of αr. The solid curve shows the fit to the average of all eight sets using the analytic representation, $N=N_0[1-\exp(-\alpha r)]$. Inset: N/N_0 for small αr.

eight systems. What is striking about this figure is that $N(\alpha r)/N_0$ is a universal function of αr that is represented by Eq. (8). Furthermore, N determined from specific heat (γ) is identical to that calculated from $(dH_{c2}/dT)|_{T_c}$ since some of the data were obtained from one of these quantities while the remainder were obtained from the other quantity. Thus the equivalence of the two definitions as well as the universal shape indicate a very strong confirmation of the calculation of N based on the Landau theory given in Appendix B. It is clear that near the MIT, the slope is linear in r, and that for larger values of r, the density of states becomes nonlinear and ultimately approaches the pure limit, N_0, when $\alpha r\sim 4$. The deviation of N from linearity provides a crude estimate of αr_0, which defines the boundary between the PCR and the FLR. From the inset to Fig. 4(b), we see that this boundary occurs at $\alpha r_0\sim 0.4$. Inspection of the $T_c(\alpha r)$ curves, shown for example in Fig. 1, indicates that practically the whole $T_c(\alpha r)$ curve falls in the region defined by $\alpha r>0.4$ and thus nearly the whole curve falls in the FLR.

The behavior of $T_c(\alpha r)$ was subsequently analyzed by fitting Eq. (9), with $\delta=1$, to the data. This fitting was carried out for all nine of the systems defined above, whose behavior illustrates the full range of T_c enhancement. These results are shown in Fig. 1. The numerous points (shown as solid dots in the figures), particularly for the Nb-Ti system, precisely define the function for $T_c(r)$ over its complete range—from the MIT to the pure limit. The solid curves in each figure represent the fit of Eq. (9) to the data. The parameters l_{TF}, q_c, and a were varied and their fitted values appear in Table III. For comparison, the values for the first two parameters for the host metal also included in the same table. The agreement is quite good.

From the experimental values of $T_c(\alpha r)$ and $N(\alpha r)$, values of $V(\alpha r)$ were calculated by inverting Eq. (9a). These data as well as theoretical fits using Eqs. (9b) and (9c) (solid lines) are shown in Fig. 4. Note that $V(\alpha r)$ for each system starts at a value of $V_0=(4\pi e^2)/(k_{TF}^2+q_c^2)$ in the pure limit (large r) and increases to a value $V(0)=(4\pi e^2)/(q_c^2)$ at $\alpha r=0$, which is seen to be the unscreened potential. By definition, $V(0)$ is greater than V_0. $V(0)$ often exceeds 2 eV.The fits to the data are quite good and thus the veracity of using a screened Coulomb potential to model enhanced superconductivity in alloys is confirmed. Note that, unlike the $T_c(\alpha r)$ curves, which showed a definite trend with the parameter a, there is no particular trend apparent for $V(\alpha r)$. A second point to note is that the amplitudes of the interaction potential are well defined and specific.

Using Eqs. (10), we generated $T_{c\ max}$ curves for several hosts. The results are shown in Figs. 5(a)–5(d). The first panel shows $T_c(\alpha r)$ as a is varied for a superconductor with $T_{c0}\sim 8$ K. $T_c(\alpha r)$ for different values of a and for different superconductors is shown in Fig. 1. Figure 5(b) shows $T_{c\ max}$ for several hosts as a function of a. For the limit $a=0$, $V=V_0$, and thus $T_{c\ max}=T_{c0}$. For the limit $a\to\infty$, $V=V(0)$, and $T_{c\ max}=T_c(0)$. It is clear that the curves look very similar, although they differ in the vertical offset and scaling of the vertical axis. In Fig. 5(c), a comparison is made between the predicted values of $T_{c\ max}$ for the host, Mo, and values of $T_{c\ max}$ found for the following alloys: Mo-Nb, Mo-Si, Mo-Ge, Mo-Ti, and Mo-Re. Furthermore, a scan of all the Mo alloys in the literature (with unknown a) shows that there is no alloy whose T_c exceeds 14 K, a value that is close to the maximum predicted [10 K, Fig. 5(c)]. The agreement for Mo systems is thus quite reasonable. Unfortunately, the data in the literature are insufficient to test these predictions for other alloy systems. We do note, however, that Eq. (10a) predicts that $T_{c\ max}$ for Pb should attain a value of 35 K, whereas the maximum T_c reported for any Pb alloy is only 11 K. One possible explanation is that, for some (unknown) reason a never exceeds 1 for this system. Finally, it is possible to plot $T_{c\ max}/T_{c0}$ for all the systems and compare those data with predictions. This is done in Fig. 5(d), and again, the agreement is good.

From the fitted values of a and α, the quantity l_s may be

TABLE II. Parameters obtained from fitting data for N by Eq. (8).

Material	N_0 host (states eV^{-1})	N_0 (states eV^{-1})	dN_0 (states eV^{-1})	σ_c [$(\Omega$ cm$)^{-1}$]	$d\sigma_c$ [$(\Omega$ cm$)^{-1}$]	α	$d\alpha$
Nb-Ti	1.62	1.62	0.10	3 500	1000	0.35	0.03
W-Si	0.26	0.25	[a]	500[b]			
Nb_3Sn	2.00	0.90	0.01	22 000	1000	0.03	0.01
V-Ti	1.92	1.90	0.10	4 800	500	0.37	0.04
Ta-Ti	1.24	1.20	0.10	9 200	1000	1.80	0.10
Re-Mo	0.50	0.51	0.01	4.4[c]	0.50[c]	0.30	0.03
Mo-Nb	0.45	0.45	[a]				
Mo-Si	0.45	0.44	[a]	3 000	1000	3.10	0.04
Mo-Ge	0.45	0.44	[a]	5 800	850	6.10	0.06
Mo-Ti	0.45	0.44	[a]	5 800	500	6.10	0.60

[a]This parameter was not varied during the fit, but fixed at the calculated value.

[b]The value for σ_c for W-Si was obtained by a different method (see Ref. 9). Thus there are no values for α and $d\alpha$.

[c]These parameters are for x_c and dx_c, since the density of states was only given as a function of concentration, x.

evaluated for each system. A sample is shown in Fig. 6 for four of them. Note that l_s has the appropriate limits and furthermore that l_s only changes by a factor of 3 as each system traverses the distance from pure metal to insulator. Thus, it is demonstrated that the screening length has a very reasonable behavior as αr spans the range from good conductor to insulator. Indeed, the point of Figs. 3, 4, and 6 is to demonstrate that all the physical quantities vary over very reasonable ranges as T_c undergoes the very dramatic behavior shown in Fig. 1. Furthermore, as these figures show, the significant changes occur over a well-defined region ($0 < \alpha r < 4$) in the vicinity of the MIT.

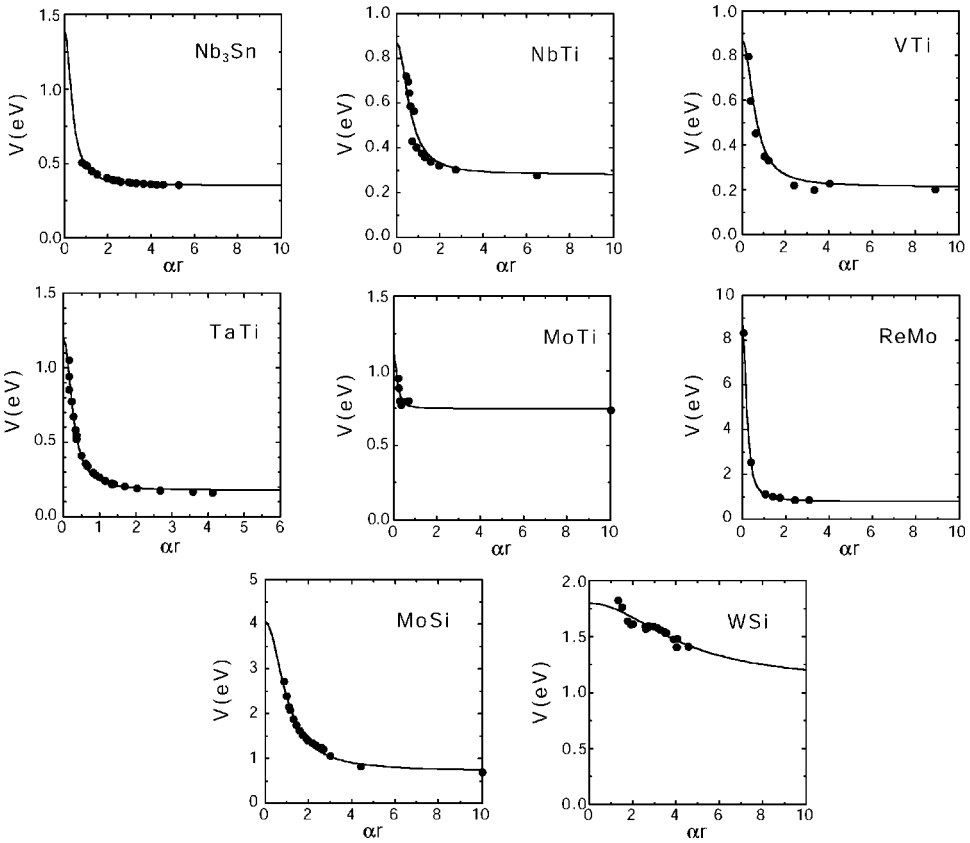

FIG. 4. The experimentally determined interaction potential, V versus αr for eight of the systems considered in this study. The data points (solid circles) were calculated from measured values of T_c and N using the McMillan equation for T_c. The solid curves are fits of the analytic expression for the screened Coulomb potential (see text).

TABLE III. Parameters obtained from fitting data for T_c using Eq. (9a).

Material	l_{TF} host (Å)	l_{TF} fit (Å)	dl_{TF} (Å)	q_c host (Å)	q_c fit (Å)	dq_c (Å)	a fit (Å)	δa (Å)	$T_{c\,max}/T_{c0}$
Nb-Ti	0.85	0.72	0.02	1.27	1.07	0.04	0.69	0.05	1.11
W-Si	2.10	1.70	[a]	0.78	0.75	[a]	24.1	1.5	333
Nb_3Sn	0.76	0.89	0.02	0.79	1.09	0.04	0.01	0.005	1.00
V-Ti	0.77	0.75	0.03	1.56	1.61	0.02	1.50	0.05	1.38
Ta-Ti	0.96	1.03	0.05	1.22	1.30	0.01	2.50	0.1	2.50
Re-Mo	1.51	1.43	0.08	0.89	0.96	0.01	11.0	2.0	6.50
Mo-Nb	1.60	1.60	[a]	0.87	0.92	0.01	0.01	0.001	1.00
Mo-Si	1.60	1.60	[a]	0.87	0.95	0.05	17.0	5.0	6.00
Mo-Ge	1.60	1.62	0.07	0.87	0.92	[a]	15.0	2.0	6.00
Mo-Ti	1.60	1.60	[a]	0.87	0.92	0.01	6.00	1.0	4.00

[a]This parameter was not varied during the fit, but fixed at, or near, the calculated value.

V. INTERPRETATION AND DISCUSSION

A. Enhanced T_c

Enhanced T_c depends on two factors. The possible range of $T_{c\,max}$ is determined by the range of V_0 and $V(0)$; the larger the difference between these two parameters [see Eq. (5) and Fig. 5], the larger the possible value of $T_{c\,max}$. Indeed, using the appropriate definitions, $V(0) = V_0[1+(k_{TF}/q_c)^2]$, so that the range is seen to increase when q_c is small. The actual value of $T_{c\,max}$ is determined by the maximum value of the product NV, which has been amply shown to occur at $\alpha r \sim 3$. The corresponding value of $T_{c\,max}$ is given by Eqs. (9a) and (9b), which depend explicitly on the phenomenological fitting parameter, a. In general, $T_{c\,max}$ increases as a [see Fig. 5(b)]. In view of the importance of this parameter, it would strengthen the utility of the EMA model if the parameter a could be related to a measurable quantity.

In this section we will suggest that this parameter can be deduced from a known, measured quantity. Far from the MIT, the well-known kinetic expression for the conductivity applies in three dimensions,

$$\sigma = \frac{ne^2\tau}{m} = \left(\frac{e^2}{3\pi^2\hbar}\right)(k_F l)k_F . \tag{11}$$

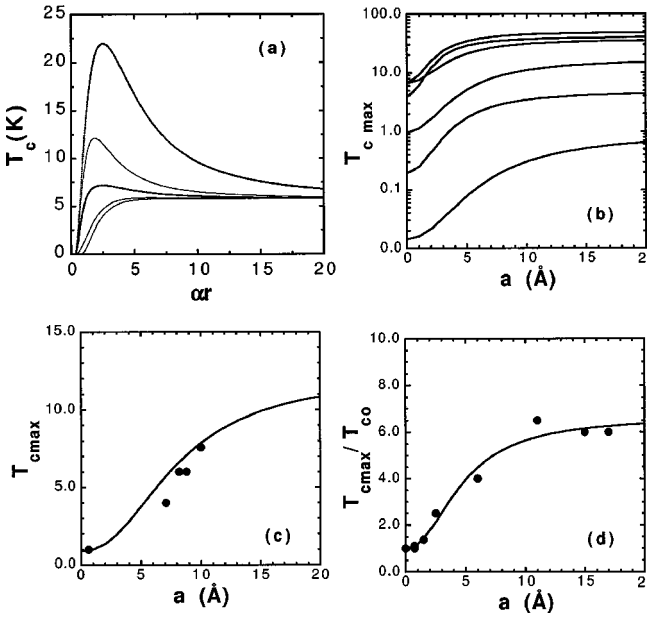

FIG. 5. (a) Calculation of $T_c(ar)$ as a function of the enhancement parameter, a. Reading from the bottom to the top, a is 0, 0.7, 1.5, 2.5, and 6.0. (b) A calculation of the maximum T_c for several systems as a function of the enhancement parameter, a. Proceeding from the lowest to the highest, they are W, Ti, Mo, V, Pb, and Nb. (c). Calculated curve for the maximum T_c of Mo alloys with five data points from the following systems (reading left to right): Mo-Nb, Mo-Ti, Mo-Ge, Mo-Si, and Mo-Re. (d). $T_{c\,max}/T_{c0}$ for all the alloy systems studied here.

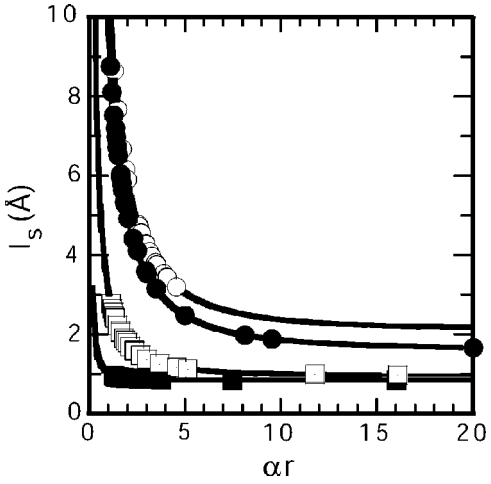

FIG. 6. The screening length, l_s, as a function of αr for four of the systems studied here. Reading from the lowest to the highest, the systems are: Nb-Ti, Ti-Ta, Mo-Ti, and W-Si. The curves represent the bridging function [Eq. (6)] proposed in the text.

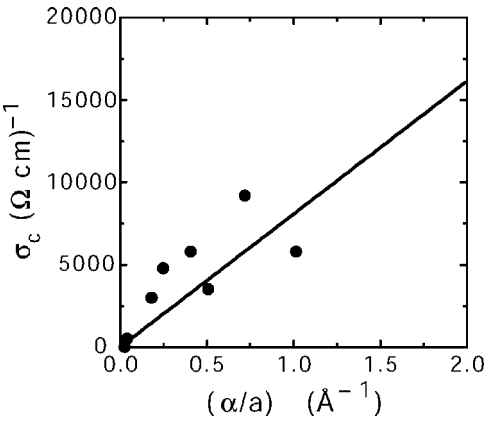

FIG. 7. Plot of σ_c versus the inverse of the enhancement parameter α/a.

Near the MIT this expression applies for the bare, unrenormalized, conductivity; i.e., the conductivity at the microscopic length scale. This was the basis of the rationale for using $\sigma(300\ \mathrm{K})$ in Eq. (1) since the renormalization is cut off on microscopic length scales at high energy.[11] Now σ_c is defined by the condition that the mean free path, l, becomes very small and equal to a/α, which is on the order of the lattice spacing, but not necessarily equal to it. At criticality, $k_F l \sim \pi$, $l \sim a/\alpha$, and $k_F \sim \pi\alpha/a$. Thus,

$$\sigma_c \approx \left(\frac{e^2}{3\pi^2\hbar}\right)\left(\frac{\pi^2}{a/\alpha}\right) \approx \frac{8200}{a/\alpha}(\Omega\ \text{Å})^{-1}. \tag{12}$$

Hence, the parameter a/α is related to a measurable quantity. To test this prediction, we plot in Fig. 7 values of σ_c determined from $N(\sigma)$ data versus α/a determined from fits of $T_c(\alpha r)$ for the same system. The correlation appears to hold, although with moderate scatter. The slope is 8100, well within 10% of the predicted value. This small discrepancy is not surprising since $\sigma(300\ \mathrm{K})$ only approximates σ_{bare}.[11]

B. Exceptions

The EMA model is not a''theory of everything'' for superconductivity. First, it applies only to systems exhibiting a MIT. Thus there are many exceptions. For instance, isoelectronic transition-metal alloys, e.g., Nb-Ta,[47] Nb-V,[47] Ti-Zr,[46] Ta-V,[48] and Os-Ru,[49] do possess phase lines, $T_c(x)$, but since there is no MIT, the EMA model clearly does not apply to these systems. Indeed, a model based upon the effect of alloying on λ rather than upon the presence of an MIT, has been developed by Weinkauf and Zittartz,[50] which accounts quite well for the phase lines of these materials.[51] Second, granular films [notably Al (Ref. 52)] even have a MIT, but the samples tend to be inhomogeneous, which makes an unknown contribution to the conductivity axis and thus renders the EMA model inapplicable. Films made from Pb (Ref. 53) and Bi (Ref. 54) also have a MIT, and $T_c(x)$ is fitted by the EMA model. A systematic study of this promising area will be reported elsewhere.

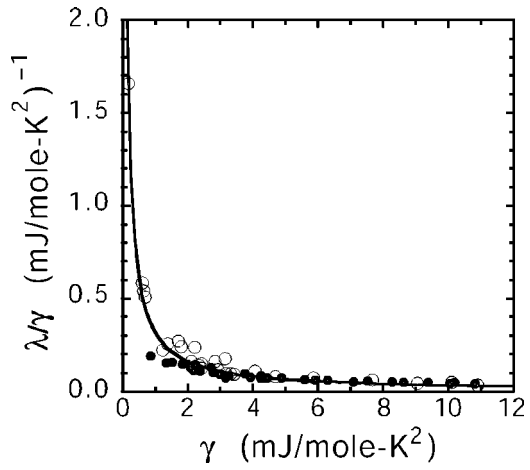

FIG. 8. λ/γ versus γ for the elements (open circles) (as given in Table I) and for several transition metal elements and alloys (solid circles) [from (Ref. 62)]. The solid curve is a fit to the combined data sets by a screened Coulomb potential (see text).

VI. CONCLUSION

Using the Landau theory for interacting fermions, in which the quasiparticles interact via a screened Coulomb potential, we derived expressions for the BCS interaction potential, V, and the single-particle density of states, N, as a function of distance from the metal-insulator transition. Then N and V were incorporated into the McMillan expression to provide an explicit expression for T_c. We systematically compared these predictions with data available in the literature for several superconducting systems: Mo-Ge, Mo-Nb, Mo-Si, Mo-Re, Mo-Ti, Ti-V, Ti-Ta, Nb-Ti, W-Si, and Nb_3Sn.

Data for $N(r)$, obtained either from experimental determinations of γ or from $(dH_{c2}/dT)|_{T_c}$, were successfully fitted by the function given by Eq. (8) (Fig. 3). Experimental values for $V(r)$, obtained by inverting the McMillan T_c equation and using measured values of T_c and N, were successfully fitted by Eq. (5) (Fig. 4). Experimental data for T_c were then successfully fit by Eq. (9a) (Fig. 1) for these systems. The dependence of the screening length for several systems (Fig. 6) emphasizes the fact that changes by only a factor of 3 in order to induce the profound changes in $V(r)$ and T_c. Other ramifications of this extension of the Morel-Anderson model, such as the maximum T_c (Fig. 5) and definition of one of the parameters (Fig. 7), are demonstrated. The EMA model may also account for some correlations made early on in the history of superconductivity (Figs. 8 and 9).

Thus the EMA model is quite robust, for it accounts extremely well for data taken over the complete range of metallic behavior for an alloy system, from the pure metal to the MIT. Indeed, the EMA model successfully predicts the complete phase line $T_c(r)$ that separates the normal from the superconductive phases. Furthermore, all the parameters appearing in the equations derived by the model are given in terms of quantities that are measured independently. It is thus a model that can be used to guide research in the search for new superconducting materials. Nevertheless, it is a phenomenological model that assuredly applies in the pure limit, but

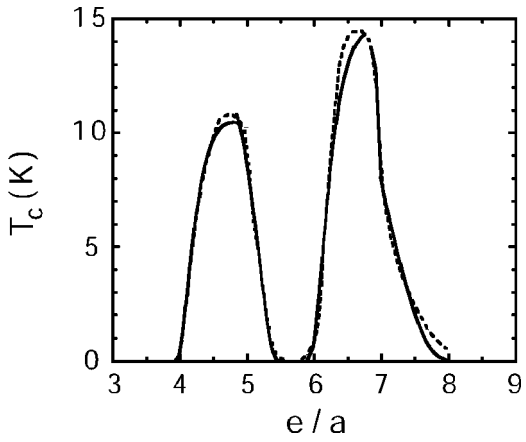

FIG. 9. T_c as a function of e/a for the $3d$, $4d$, and $5d$ elements and alloys (dashed curve). Fit using EMA model (solid curve).

whose applicability becomes increasingly suspect as the system approaches the MIT. How can we reconcile the success of the EMA model over the complete range with the dissolution of the Fermi liquid framework near the MIT? We believe that the EMA model is a''roadmap,'' which, by requiring its bridging functions to match Fermi liquid theory at one extreme and scaling theory at the other, is successful. It is hoped that its success will inspire an effort to carry out the calculation of N, V, and T_c using a proper microscopic theory.

ACKNOWLEDGMENTS

We thank V. Z. Kresin for a careful reading of the theory parts of this article and for several suggestions. We thank J. Claassen for a critical reading of this manuscript and for numerous suggestions. We benefited from insightful discussions with I. Mazin, A. Gulian, and V. Gurevich. We also thank M. Adams and D. Larbalestier for access to documents in the private library of the Applied Superconductivity Center at the University of Wisconsin. L.D.C. acknowledges support by the U.S. Department of Energy.

APPENDIX A: CALCULATION OF T_c FOR THE PURE LIMIT

The BCS theory[55] was the first to successfully account for the properties of pure superconductors, as well as for alloy systems $A_{1-x}B_x$, as long as the doping concentration, x, is small.[56] It posits a bold approximation: that a constant interaction V_0 may be substituted for the complex interaction between two conduction electrons, which in reality is the sum of an instantaneous Coulomb repulsion and an attractive, time-dependent electron-phonon interaction. This interaction potential V_0 is left as a phenomenological parameter to be adjusted by fitting to experimental data. (We will adopt the notation that a subscript 0 will refer to the pure material.) Among the predictions of the BCS theory is an expression for the superconductive energy gap, Δ,

$$\Delta = \int_0^{\hbar\omega_D} V_0 \Delta(E) \left[\frac{1-2f(E)}{(E^2-\Delta^2)^{1/2}} \right] dE. \tag{A1}$$

From the requirement that $\Delta=0$ at T_c, the BCS theory predicts the following equation for T_c:

$$T_c = 0.85\Theta_D \exp\left(\frac{-1}{NV_0}\right), \tag{A2}$$

where Θ_D is the Debye temperature and N is the density of states at the Fermi surface.

This expression is accurate only when NV_0 is small (weak coupling). The density of states is well defined by the theory for free electrons, which states that $N=3n/2E_F$, where E_F is the Fermi energy. Furthermore, N may also be determined by two independent experiments: from the specific heat, where $N=0.212\gamma$ (where γ is the Sommerfeld constant) or from the slope of the upper critical magnetic field at T_c, where $N=[h\pi(dH_{c2}/dT)|_{T_c}]/16\rho_0 e^2$,[57] with ρ_0 being the resistivity in the normal state. Once T_c and N are determined by independent experiments, the BCS equation for T_c can be inverted and the experimental values for N and T_c used to calculate V_0. This has been done for several materials, but the results were not particularly interesting since the BCS theory did not calculate a theoretical value for comparison.

Several formulations of superconductivity followed the BCS theory in which V_0 was replaced by more realistic potentials. Eliashberg[58] developed the modern expression for the gap equation that is given below in simplified form,

$$\Delta(\omega_n) = \frac{\pi k_B T}{Z(\omega_n)} \sum_{\omega_{n'}}^{\infty} [\lambda D(\omega_n - \omega_{n'}) - \mu^* \Theta(E_F - \omega_{n'})] \frac{\Delta(\omega_{n'})}{|\omega_{n'}|}, \tag{A3}$$

where $\omega_n=(2n+1)\pi k_B T$, D is the phonon Green's function, Z is the renormalization factor, and Θ is the Heaviside step function. This theory is characterized by two parameters, λ and μ^*. The first corresponds to the phonon-mediated interaction. The second corresponds to the repulsive Coulomb interaction. They are defined by the equations

$$\lambda = 2\int \frac{g(\Omega)F(\Omega)}{\Omega} d\Omega, \tag{A4a}$$

$$\mu = 2\int V(\Omega) d\Omega, \tag{A4b}$$

where g is the square of the electron-phonon matrix element and $F(\Omega)$ is the phonon density of states. McMillan[59] solved the gap equation numerically and thereby determined a semiempirical expression for T_c:

$$T_c = 0.85\Theta_D \exp\left[\frac{-1.04(1+\lambda)}{\lambda - \mu^*(1+0.62\lambda)}\right], \tag{A5}$$

where μ^* is given by

$$\mu^* = \frac{\mu}{1+\mu \ln(E_F/k_B\Theta_D)}. \tag{A6}$$

McMillan's equation is accurate for λ as large as 1.5. Note that for small λ it reduces to the BCS expression if NV_0 is identified as $\lambda-\mu^*$.

In order to use the McMillan expression to calculate T_c for any metal, however, more specific expressions for λ and μ^* are needed. One method involves incorporating the metal into a tunnel junction, carrying out tunneling measurements, and then deconvolving the data taken to extract the quantity gF, from which λ and μ^* may be calculated from the defining integrals. Difficulties in fabricating good quality tunnel junctions have restricted application of this technique to a limited number of materials, however. An alternative path is to obtain theoretical estimates, which may be done, for example, using band theory. Unfortunately this approach is not particularly well suited for the region near the MIT. Guided by the experience of Ref. 9, which identified screening as the crucial factor in determining T_c near the MIT, we follow the model developed by Morel and Anderson, where the effect of screening is explicit. MA calculated λ and μ^* for most of the elements, expressing them in terms of the screened Coulomb potential that enters linearly into the expression for μ and quadratically via the electron-phonon interaction for λ. That is, if the Coulomb electrostatic potential is screened spatially as $V(x)=(e^2/x)\exp(-k_{TF}x)=(e^2/x)\exp(-x/l_{TF})$, then the Fourier transform $V(q,k_{TF})$ is given by

$$V(q,k_{TF})=\frac{4\pi e^2}{q^2\epsilon(q,k_{TF})}=\frac{4\pi e^2}{k_{TF}^2+q^2}. \tag{A7}$$

Here $l_{TF}=1/k_{TF}$ is the Thomas-Fermi screening length and ϵ the dielectric function. Morel and Anderson then present the following calculation of λ:

$$\lambda=2\int\frac{g(\Omega)F(\Omega)}{\Omega}d\Omega=2\left\langle\frac{g(\Omega)}{\Omega}\right\rangle\int F(\Omega)d\Omega$$
$$=\frac{2N_0^2}{q_c^2}\int_0^{q_c}\left(\frac{4\pi e^2}{k_{TF}^2+q^2}\right)^2 qdq=\frac{N_0}{q_c^2}\left(\frac{4\pi e^2}{k_{TF}^2+q_c^2}\right)=N_0V_0, \tag{A8a}$$

$$\mu=\frac{1}{2\pi^2v_F}\int_0^{q_c}V(q,k_{TF})qdq=\ln\left(1+\frac{q_c^2}{k_{TF}^2}\right)=-\ln(\lambda). \tag{A8b}$$

The steps followed by Morel and Anderson in their calculation of λ may be seen by reading Eq. (A8a) from line to line. MA use the simple matrix element $g/\Omega=(1/2N)[k_{TF}^2/(k_{TF}^2+q^2)]^2$, which is independent of Ω. Thus in line 2, this quantity is pulled outside of the integral, but it still must be averaged (angular brackets) over the angle between the phonon and electron wave vectors. In line 3, a δ function is used for $F(\Omega)$. In line 4 the integration over the angle $x=\sin(\theta/2)=(k'-k)/2k_F=q/2k_F$ (normal phonon process) from 0 to x_m is carried out.

MA set the maximum phonon momentum q_c equal to $2k_F$. MA also derived a different expression for λ for phonon umklapp processes, which is believed to be more appropriate for some of the elements. We found the introduction of this complication led to poor fits to T_c, so we used the expression for normal phonon processes. Since the dependence of λ on k_{TF} is logarithmic, and $\ln(E_F/k_B\Theta_D)$ is approximately 5, μ^* is approximately constant for the pure metals at a value of 0.15. Thus the influence of the screening on T_c is felt almost entirely via its effect on λ.

APPENDIX B: CALCULATION OF T_c FOR THE STRONGLY INTERACTING, DISORDERED FERMI LIQUID

Here we use the description of a disordered Fermi liquid developed by Altschuler and Aranov.[60] Since their seminal work remains within the confines of Fermi liquid theory, we assert that the McMillan expression for T_c still applies. What is needed, then, to predict T_c are expressions for V and N. The derivation of N given by Altschuler and Aranov starts with the formal definition,[61]

$$N=N_0/(1+d\Sigma/d\epsilon), \tag{B1}$$

where Σ is the self-energy of the quasiparticles of energy ϵ. The derivative $d\Sigma/d\epsilon$ is in turn defined by an integral that incorporates the quasiparticle interaction potential $V(q)$ (the screened Coulomb potential) and the inverse screening length k_s. Thus,

$$d\Sigma/d\epsilon=\int\frac{dq}{(2\pi)^3}\left[\frac{Dq^2}{\epsilon^2+(Dq^2)^2}\right]V(q)\frac{\partial n}{\partial\mu}$$
$$=\int\frac{dq}{(2\pi)^3}\left[\frac{Dq^2}{\epsilon^2+(Dq^2)^2}\right]\left(\frac{4\pi e^2}{k_s^2+q^2}\right)\frac{\partial n}{\partial\mu}, \tag{B2}$$

where D is the diffusion coefficient, k_s is defined in terms of $\partial n/\partial\mu$ by the equation

$$k_s^2=4\pi e^2(\partial n/\partial\mu), \tag{B3}$$

and the interaction potential is given by

$$V(q)=\left(\frac{4\pi e^2}{k_s^2+q^2}\right). \tag{B4}$$

Evaluation of this integral for the case where the energy is at the Fermi surface yields

$$d\Sigma/d\epsilon=\left(\frac{2e^2}{\pi\hbar^{3/2}}\right)\left[\frac{\sqrt{\epsilon_F}}{k_s^2D^{3/2}}\right]=\left(\frac{2e^5}{\pi\hbar^{3/2}}\right)\left[\frac{\sqrt{\epsilon_F}k_s}{(4\pi\sigma)^{3/2}}\right]$$
$$=\left(\frac{2e^5}{\pi\hbar^{3/2}}\right)\left[\frac{\sqrt{\epsilon_F}k_s}{[4\pi\sigma_c(r+1)]^{3/2}}\right]. \tag{B5}$$

Up to this point the derivation is accurate and based upon microscopic theory. However, the quantities N and V are defined in terms of k_s. In order to express the results in terms of the measurable coordinate r, then k_s needs to be expressed in terms of r.

Since we are not aware of a microscopic derivation of such a relation, we provide the following phenomenological

TABLE IV. $N(r)$, $V(r)$, and $k_s(r)$ for different regimes of metallic behavior.

Quantity	CR ($\alpha r \to 0$)	PCR ($\alpha r \lesssim 0.4$)	FLR (strong) ($\alpha r \gtrsim 0.4$)	FLR (weak) ($\alpha r \to \infty$)	Proposed bridging function for complete range
N		$N_0 \alpha r$	$\dfrac{N_0}{(1+\gamma k_s r^{-3/2})}$	N_0	$N_0[1-\exp(-\alpha r)]$
V	$\dfrac{4\pi e^2}{q_c^2}$		$\dfrac{4\pi e^2}{k_s^2+q_c^2}$	$\dfrac{4\pi e^2}{k_{TF}^2+q_c^2}$	$\dfrac{4\pi e^2}{k_s^2+q_c^2}$
k_s^2	$(\alpha r/a)^2$		$\dfrac{k_{TF}^2}{1+(a/\alpha r)^2}$	k_{TF}^2	$\dfrac{k_{TF}^2}{1+(a/\alpha r)^2}$

argument. First, we know the limiting values of k_s. That is, near the MIT $k_s = 1/l_s \sim r$, while in the pure limit $k_s = k_{TF}$. Furthermore, from the Landau theory for Fermi liquids, we know that $\partial n/\partial \mu = N_0/(1+F)$, where F is related to the interaction between the quasiparticles. A clue for the functional dependence of F in terms of r comes from a study of another physical system, where it was found that F diverged (and thus $k_s \to 0$) as the MIT was approached. The following expression for k_s satisfies all of the above requirements:

$$k_s^2 = 4\pi e^2(\partial n/\partial \mu) \sim \frac{4\pi e^2 N_0}{1+F} = \frac{k_{TF}^2}{1+(a/\alpha r)^2}. \quad \text{(B6)}$$

Substitution of k_s into the expressions for V and N now expresses them, and thus T_c, in terms of r for the strongly interacting Fermi liquid regime.

APPENDIX C: DEVELOPMENT OF EXPRESSIONS FOR THE FULL METALLIC RANGE

In Appendix A we developed expressions for V, N, k_s, and ultimately T_c for the weakly interacting Fermi liquid, which were based upon the Morel-Anderson analysis. In Appendix B we used the Altschuler-Aronov analysis to develop different expressions for the same quantities for the strongly interacting Fermi liquid. These functions are given in Table IV. We were unable to find similar analyses for the PCR and CR part of the metallic range. However, we know the behavior near the MIT from scaling theory and have also entered them into this table. The information provided by scaling theory is invaluable in helping to define the boundary condition for these functions at $r=0$. From this information we were able to construct a *single* function for N, which is given in the last column of Table IV, and which represents rather accurately—over the full metallic range—all the separate functions for N over their respective domains. Thus, this function acts as a ''bridging function,'' which is based piecemeal on different theories. The expression for V given in the last column is precise and represents the fact that the screened Coulomb potential is appropriate for all regimes. The McMillan expression for T_c was used with these functions to fit the phase diagrams $T_c(r)$.

The expression for k_s is purely phenomenological and defined by the two boundary conditions at $r=0$ and $r=\infty$. The three regions for metallic behavior are arranged as a function of increasing r across this table, where the boundary between the PCR and the FLR occurs for $\alpha r_0 \sim 0.4$.

APPENDIX D

The expression for T_c presented here gives insight into at least three empirical correlations for T_c which were pointed out many years ago. The first was made by Bucher *et al.*[62] They showed that the experimental values of λ for the $3d$, $4d$, and $5d$ transition-metal elements and alloys displayed a clear correlation with γ (see Fig. 32 of Ref. 63), which is reproduced here as Fig. 8. Indeed, the data points were fit quite well by the *empirical* equation

$$\lambda/\gamma = a/(1+b\gamma). \quad \text{(D1)}$$

Since $N = 0.212\gamma$, it is clear that λ/γ is actually identical to the quantity V *derived* herein. To verify this, we calculated λ/γ for the elements from the data presented in Table I and plotted it versus λ along with the Bucher data in Fig. 8. It is clear that the two data sets are identical when allowance is made for scatter. We reexpressed the equation for λ as $\lambda/\gamma = c/(d+\gamma)$ to cast it into the same functional form as $V_0 = c/(d+k_{TF}^2)$ used to fit the data shown for all the elements in Fig. 2(a). The fit to the combined data, shown as the solid line in Fig. 8, is quite good.

The second comment also applies to transition metal elements and alloys. Experiments have established that the T_c for the $3d$, $4d$, and $5d$ elements and alloys have the same, striking, two-peaked dependence on the valence per atom, e/a (see for example, Fig. 30 of Ref. 63). We display the average of T_c for the three groups in Fig. 9,[64] as shown by the dashed line, where it is clear that two maxima appear at $e/a \sim 4.8$ and 6.8, and that three minima appear at $e/a \sim 3.7$, 5.7 and 8.7. The measured values for λ for the same materials have a very similar behavior (see Fig. 29 of Ref. 63), whereas Θ_D and V_0 are almost constant (Table VII and Fig. 28, respectively, of Ref. 63). The behavior shown in Fig. 9 may be explained quite easily by the EMA model if the three minima in γ and T_c are interpreted as being caused by three regions where the MIT occurs. Note that the minima appear at values of e/a that are about halfway between the pure metal values of e/a. This is precisely where ρ would be the largest for a classic AB alloy system [since resistivity

varies[65] as $x(1-x)$], and thus where each MIT is located. Now the conductivity of an alloy varies as the inverse square of the valence difference between the host and dopant metals,[66] thus $\sigma \sim (e/a)^{-2}$. Using the definition of r given by Eq. (1), then $r=[(e/a)_c/(e/a)]^2-1$, where the critical values $(e/a)_c$ occur at 3.7, 5.7 and 8.7. The dashed curve in Fig. (8) was fitted by Eq. (10a) with this definition of r, and the resulting fit is shown as the solid line. The EMA model provides a particularly facile explanation of this striking figure.

The third comment concerns the correlation established by Testardi and collaborators:[7] that T_c is a universal function of the residual resistance ratio$=\rho(300\ \mathrm{K})/\rho(T_c) = \sigma(T_c)/\sigma(300\ \mathrm{K})$. To the extent that the Testardi correlation simply points out that T_c decreases for many materials when they become dirty, then we identify this case as that given by the EMA model when there is no enhancement.

*Electronic address: soulen@anvil.nrl.navy.mil

[1] B.W. Roberts, J. Phys. Chem. Ref. Data **5**, 581 (1976).

[2] See, for example, The Proceedings of the Conference on Synthetic Metals, Les Arcs, France, 1982, J. Phys. (Paris) Colloq. **44**, C-3 (1983).

[3] See, for example, Thomas P. Sheahen, *Introduction to High-Temperature Superconductivity* (Plenum Press, New York, 1994).

[4] See, for example, M. Cohen, in *Superconductivity*, edited by R.D. Parks (Marcel Dekker, New York, 1969), Chap. 12.

[5] See, for example, O. Gunnersson, Rev. Mod. Phys. **69**, 575 (1997).

[6] See, for example, B.T. Matthias, Phys. Rev. **97**, 74 (1955).

[7] See, for example, L.H. Testardi, J.M. Poate, and H.J. Levinstein, Phys. Rev. B **15**, 2570 (1977).

[8] P. Morel and P.W. Anderson, Phys. Rev. **125**, 1263 (1962).

[9] M.S. Osofsky, R.J. Soulen, Jr., J.H. Claassen, G. Trotter, H. Kim, and J.S. Horwitz, Phys. Rev. Lett. **87**, 197004 (2001).

[10] The correlation length discussed here is not the superconducting coherence length, which is often identified by the same symbol.

[11] M. Osofsky, H. Tardy, M. LaMadrid, and J.M. Mochel, Phys. Rev. B **31**, 4715 (1985); **32**, 2101 (1985).

[12] G. Hertel, D.J. Bishop, E.G. Spencer, J.M. Rowell, and R.C. Dynes, Phys. Rev. Lett. **50**, 743 (1983).

[13] P.W. Anderson, Phys. Rev. **109**, 1492 (1958).

[14] N.F. Mott, Philos. Mag. **24**, 935 (1974).

[15] D. Belitz and T.R. Kirkpatrick, Rev. Mod. Phys. **66**, 261 (1994).

[16] S. Yoshizumi, D. Mael, T. H. Geballe, and R. L. Greene, in *Localization and Metal-Insulator Transitions*, edited by H. Fritzsche and D. Adler (Plenum Press, New York), p. 77.

[17] D.J. Bishop, E.G. Spencer, and R.C. Dynes, Solid-State Electron. **28**, 73 (1985).

[18] N. Nishida, T. Furubayashi, M. Yamaguchi, K. Morigaki, and H. Ishimoto, Solid-State Electron. **27**, 81 (1985).

[19] T.R. Kirkpatrick and D. Belitz, Phys. Rev. Lett. **70**, 974 (1993).

[20] W.L. McMillan, Phys. Rev. B **24**, 2739 (1981).

[21] T.R. Kirkpatrick and D. Belitz, Phys. Rev. Lett. **68**, 3232 (1992).

[22] A.M. Finkel'stein, Physica B **197**, 636 (1994).

[23] C. Grimaldi, L. Pictronero, and S. Strassler, Phys. Rev. Lett. **75**, 1158 (1995).

[24] F. Marsiglio and J.E. Hirsch, Phys. Rev. B **49**, 1366 (1994).

[25] R.A. Hein, J.W. Gibson, and R.D. Blaugher, Rev. Mod. Phys. **36**, 149 (1964).

[26] E. Bucher, F. Heiniger, J. Muheim, and J. Muller, Rev. Mod. Phys. **36**, 146 (1964).

[27] M. V. Sadovskii, *Superconductivity and Localization* (World Scientific, Singapore, 2000).

[28] E.G. Astrakharchik and C.J. Adkins, Phys. Rev. B **50**, 13 622 (1994).

[29] O. Bourgeois, A. Frydnan, and R.C. Dynes, Phys. Rev. Lett. **88**, 186403 (2002).

[30] David Pines, Phys. Rev. **109**, 280 (1958).

[31] P. G. de Gennes, *Superconductivity in Metals and Alloys* (W. A. Benjamin, New York, 1966).

[32] Qimiao Si and C.M. Varma, Phys. Rev. Lett. **81**, 4951 (1998).

[33] G. Kothur, Sahana Murthy, and M.J. Rozenberg, Phys. Rev. Lett. **89**, 046401 (2002).

[34] S.C. Dultz and H.W. Jiang, Phys. Rev. Lett. **84**, 4689 (2000).

[35] S. Ilani, A. Yacoby, D. Mahlu, and Hadras Shtrikman, Science **292**, 1354 (2001).

[36] M.S. Osofsky, R.J. Soulen, Jr., J.H. Claassen, G. Trotter, H. Kim, and J. Horwitz, Phys. Rev. B **66**, 020502(R) (2002).

[37] Lance Cooley, Peter Lee, and David Larbalestier, in *Handbook of Superconducting Materials*, edited by David A. Cardwell and David S. Ginley (Institute of Physics, London, 2003).

[38] A. Mani, L.S. Valdhyanathan, Y. Hariharan, M.P. Janawadkar, and T.S. Radhakrishnan, Cryogenics **36**, 937 (1996).

[39] James Charles McKinnell, Ph.D. thesis, University of Wisconsin, 1990.

[40] J.K. Hulm and R.D. Blaugher, Phys. Rev. **123**, 1569 (1961).

[41] A. K Ghosh and Myron Strongin, *Superconductivity in d- and f-band Metals*, edited by D.H. Douglass (AIP, NY, 1972), pp. 305–315.

[42] W.L. Bond *et al.*, Phys. Rev. Lett. **15**, 260 (1965).

[43] S. Kondo, J. Mater. Res. **7**, 853 (1992).

[44] S. Kubo, J. Appl. Phys. **63**, 2033 (1988).

[45] F.J. Morin and J.P. Maita, Phys. Rev. **129**, 1115 (1963).

[46] E. W. Collings, *A Sourcebook of Titanium Alloy Superconductivity* (Plenum Press, New York, 1983).

[47] T.G. Berlincourt and R.R. Hake, Phys. Rev. **131**, 140 (1963).

[48] T.H. Geballe, Rev. Mod. Phys. **35**, 134 (1964).

[49] O. Rapp, Solid State Commun. **9**, 1 (1971).

[50] A. Weinkauf and J. Zittartz, J. Low Temp. Phys. **18**, 229 (1975).

[51] A. Weinkauf and J. Zittartz, Solid State Commun. **14**, 365 (1974).

[52] R.C. Dynes and J.P. Garno, Phys. Rev. Lett. **46**, 137 (1981).

[53] Myron Strongin, R.S. Thompson, O.F. Kammerer, and J.E. Crow, Phys. Rev. B **1**, 1078 (1970).

[54] D.B. Haviland and A.M. Goldman, Phys. Rev. Lett. **62**, 2180 (1989).

[55] J. Bardeen, L.N. Cooper, and J.R. Schrieffer, Phys. Rev. **108**, 1175 (1957).

[56] P.W. Anderson, J. Phys. Chem. Solids **11**, 26 (1959).

[57] N.R. Werthamer, E. Helfand, and P.C. Hohenberg, Phys. Rev. **147**, 295 (1966).

[58] G.M. Eliashberg, Zh. Éksp. Teor. Fiz. **38**, 966 (1960) [Sov. Phys. JETP **11**, 696 (1960)].
[59] W.L. McMillan, Phys. Rev. **167**, 331 (1968).
[60] B.L. Altschuler and A.G. Aronov, Solid State Commun. **39**, 115 (1979); Zh. Éksp. Teor. Phys. **77**, 2028 (1979) [Sov. Phys. JETP **50**, 968 (1979)].
[61] P. Lee and T.V. Ramakrishnan, Rev. Mod. Phys. **57**, 287 (1985).
[62] E. Bucher, F. Heiniger, J. Muller, and J. L. Olsen, in *Proceedings of the Low Temperature Conference, LT9*, edited by J. G. Daunt *et al.* (Plenum Press, New York, 1965), Part A, p. 616.
[63] *Superconductivity*, edited by R. D. Parks (Marcel Dekker, New York, 1969).
[64] M.M. Collver and R.H. Hammond, Phys. Rev. Lett. **30**, 92 (1973).
[65] C.H. Johansson and J.O. Linde, Ann. Phys. (Leipzig) **25**, 1 (1936).
[66] J.M. Ziman, *Electrons and Phonons* (Oxford University Press, London, 1960), p. 428.